Title	Characterization of site-specific GPS errors using a short-baseline network of braced monuments at Yucca Mountain, southern Nevada.
Author(s)	Hill, Emma M.; Davis, James L.; Elo´segui, Pedro.; Wernicke, Brian P.; Malikowski, Eric.; Niemi, Nathan A.
Citation	Hill, E. M., Davis, J. L., Elo´segui, P., Wernicke, B. P., Malikowski, E., & Niemi, N. A. (2009). Characterization of site-dependent GPS errors using a short-baseline network of braced monuments at Yucca Mountain, southern Nevada. Journal of Geophysical Research,114, 1-13.
Date	2009
URL	http://hdl.handle.net/10220/8210
Rights	© 2009 by the American Geophysical Union (AGU).This paper was published in Journal of Geophysical Research and is made available as an electronic reprint (preprint) with permission of (AGU). The paper can be found at DOI: [http://dx.doi.org/10.1029/2008JB006027]. One print or electronic copy may be made for personal use only. Systematic or multiple reproduction, distribution to multiple locations via electronic or other means, duplication of any material in this paper for a fee or for commercial purposes, or modification of the content of the paper is prohibited and is subject to penalties under law.

Characterization of site-specific GPS errors using a short-baseline network of braced monuments at Yucca Mountain, southern Nevada

Emma M. Hill,[1] James L. Davis,[1] Pedro Elósegui,[2] Brian P. Wernicke,[3] Eric Malikowski,[1] and Nathan A. Niemi[4]

[1] We use a short-baseline network of braced monuments to investigate site-specific GPS effects. The network has baseline lengths of $\sim$10, 100, and 1000 m. Baseline time series have root mean square (RMS) residuals, about a model for the seasonal cycle, of $0.05-0.24$ mm for the horizontal components and $0.20-0.72$ mm for the radial. Seasonal cycles occur, with amplitudes of $0.04-0.60$ mm, even for the horizontal components and even for the shortest baselines. For many time series these lag seasonal cycles in local temperature measurements by $23-43$ days. This could suggest that they are related to bedrock thermal expansion. Both shorter-period signals and seasonal cycles for shorter baselines to REP2, the one short-braced monument in our network, are correlated with temperature, with no lag time. Differences between REP2 and the other stations, which are deep-braced, should reflect processes occurring in the upper few meters of the ground. These correlations may be related to thermal expansion of these upper ground layers, and/or thermal expansion of the monuments themselves. Even over these short distances we see a systematic increase in RMS values with increasing baseline length. This, and the low RMS levels, suggests that site-specific effects are unlikely to be the limiting factor in the use of similar GPS sites for geophysical investigations.

1. Introduction

[2] The Global Positioning System (GPS) is now being used to measure not only ground deformations at the level of $\leq$1 mm, but also transient and/or high-rate signals that occur over relatively short periods of time [e.g., *Dragert et al.*, 2001; *Lowry et al.*, 2001; *Ozawa et al.*, 2003; *Larson et al.*, 2003; *Davis et al.*, 2006; *Freed et al.*, 2007]. It is therefore important that we understand the degree to which systematic errors and unmodeled local effects can contribute to both time- and space-dependent signals in the GPS time series. However, despite the fact that the first GPS satellite was launched around three decades ago, we still do not have a reliable and high-precision error budget for this technique.

[3] One obstacle to obtaining this precise error budget has been the difficulty we face in isolating real, nonlinear motions of the sites from errors in the phase models. An example in the former category is the so-called "monument motion" (discussed below), while examples for the latter include positioning errors caused by multipath (also discussed below), antenna phase center variations [*Elósegui et al.*, 1995; *Park et al.*, 2004], unmodeled atmospheric effects [e.g., *Davis et al.*, 1985; *Treuhaft and Lanyi*, 1987; *Kedar et al.*, 2003], and satellite orbit errors [e.g., *Bauerśíma*, 1983]. While some of these errors (e.g., atmospheric effects and satellite orbit errors) will have some degree of cancelation over shorter intersite distances, others are noncanceling, site-specific effects (e.g., monument motion and local multipath errors). Generally, both types of effect are lumped together and termed "errors." In this paper we follow this convention, but are interested in separating the different types.
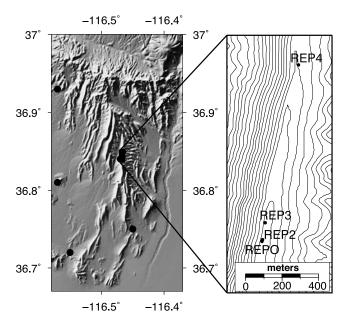
[4] Specifically, to better isolate site-specific effects we constructed a network of stations with very short intersite distances, to take advantage of this idea that errors associated with larger-scale phenomena will mostly cancel between stations. This network is an expansion of the existing Basin and Range Geodetic Network (BARGEN) [*Wernicke et al.*, 2000, 2004], and is located along the crest of Yucca Mountain, southern Nevada (Figure 1) in a position directly above the nation's only proposed civilian nuclear waste repository site. The network takes advantage of an older site (REP0), which was built in 1999, plus three additional sites (REP2, REP3, and REP4), installed in 2006 and spaced at

[1]Harvard-Smithsonian Center for Astrophysics, Cambridge, Massachusetts, USA.
[2]Institute for Space Sciences, Barcelona, Spain.
[3]Division of Geological and Planetary Sciences, California Institute of Technology, Pasadena, California, USA.
[4]Department of Geological Sciences, University of Michigan, Ann Arbor, Michigan, USA.

Figure 1. Location of the GPS network at Yucca Mountain, southern Nevada. Black dots indicate BARGEN GPS stations. Contours on the detailed map represent height and are plotted with a 20 m interval.

~10, ~100, and ~1000 m north of REPO, respectively (Figure 1). The four GPS sites have nearly identical instrumentation and setup configuration (Table 1), which is similar to that of other BARGEN sites and includes all braced monuments. However, to assess any possible effects of deep versus shallow anchoring of the monuments, site REP2 is only anchored to a depth of 3 m, rather than the 10 m of the other sites. The shallow-braced design couples a tripod-like configuration, including one vertical leg and four legs inclined 35° from vertical, directly to the upper 3 m of the ground. The deep-anchored monuments include one vertical leg and three inclined legs. In contrast to the shallow-braced design, the monument is mechanically isolated from the surrounding bedrock by an ~1 cm thick layer of foam insulation in the upper 5 m. It is only directly coupled to the ground from 5 to 10 m depth. (Figure S1 in the auxiliary material is a diagram of the two different monument types.[1]) Here we use data acquired between 2006.2 and 2009.0 (about 2.7 years in total) to characterize site-specific effects for these four monuments, paying particular attention to monument motion, thermal expansion, and multipath.

[5] The term "monument motion" has been used to describe both processes whereby the position of the antenna is cumulatively and/or randomly displaced over time (we will refer to this as "monument wander" in this paper), and processes which result in a seasonal pattern of deformation [e.g., *Langbein and Johnson*, 1997]. Monument wander could be the result of factors such as long-term weathering of rock and soil local to the monument [*Langbein and Johnson*, 1997], while the seasonal component is usually related to changes in groundwater [e.g., *Langbein et al.*,

1990; *Bawden et al.*, 2001; *Finnegan et al.*, 2008] and/or temperature [e.g., *Dong et al.*, 2002; *Romagnoli et al.*, 2003].

[6] Monument wander is often assumed to behave as a random walk process, meaning that displacement relative to the original position is expected to increase as the square root of time and the spectral density will take the form $1/f^2$ (where f is the temporal frequency) [*Johnson and Agnew*, 1995; *Langbein and Johnson*, 1997]. Previous studies have demonstrated the difficulty in quantifying the possible effects of this random walk motion on GPS results, stemming both from problems with the shortness of available time series and the fact that other sources of noise usually obscure any evidence of random walk [e.g., *Zhang et al.*, 1997; *Mao et al.*, 1999; *Williams et al.*, 2004; *Beavan*, 2005]. These studies have generally found their GPS results to be best fit by either a white noise, or white noise plus flicker noise, model.

[7] Thermal expansion could occur both of the GPS monument itself and of the ground to which it is attached. In terms of monument thermal expansion, *Romagnoli et al.* [2003] estimated that thermal expansion could lead to ~1 mm of seasonal height variation at their monument (a concrete pillar set 7 m deep into the ground, with a 0.6 m steel pole on top of this to support the antenna). For bedrock thermal expansion, *Dong et al.* [2002] used a half-space heat conduction model to estimate that ≤0.5 mm of vertical motion may be possible, with a phase of annual position variation ~ 45 days after the phase of local annual temperature variation. *Prawirodirdjo et al.* [2006] used a model that included an elastically decoupled upper layer over a uniform elastic half-space to model thermoelastic strain in horizontal GPS time series for a number of stations in the Southern California Integrated GPS Network (SCIGN). They used the phase delay between seasonal cycles in the temperature and GPS data to infer the depth of the decoupled layer, which has the effect of delaying and attenuating the temporal variations of the surface temperature, and hence the strain in the underlying half-space. For example, for one group of stations they estimated an ~39 day phase delay, which their model suggests corresponds to an unconsolidated layer of ~1 m thickness.

[8] Multipath occurs when the GPS signal reflects before arriving at the antenna, resulting in a phase difference relative to the direct signal [e.g., *Axelrad et al.*, 1996]. Multipath-induced errors can appear in many forms: The annual repeat in the GPS satellite configuration could cause an approximately annually (~350 day) repeating multipath signal [*Ray et al.*, 2007]; unmodeled subdaily signals, including those from multipath, could propagate to longer-period signals [*Penna et al.*, 2007; *King et al.*, 2008]; seasonal signals could be caused by changes in the vegetation, snow pack, and surface water of the local area around the antenna [*Dong et al.*, 2002; *Larson et al.*, 2008]; and changes in multipath could appear or disappear at random as the local environment changes [*Dong et al.*, 2002]. Additional to any effects from far-field reflections, near-field signal scattering by the antenna or monument itself can also be a significant source of error [*Elósegui et al.*, 1995].

[9] The high precision of results from other BARGEN sites in this area have been demonstrated by previous studies. For example, *Davis et al.* [2003] used a "whole

_____
[1]Auxiliary materials are available in the HTML. doi:10.1029/2008JB006027.

Table 1. Site Information for the GPS Stations in This Study[a]

Station	Baseline (m)	Height (m)	Bracing Depth (m)	Substrate	Receiver Type
REPO	0	1480	10	Densely welded rhyolitic tuff	4000 SSI
REP2	10	1480	3	Densely welded rhyolitic tuff	NetRS
REP3	103	1479	10	Densely welded rhyolitic tuff	NetRS
REP4	996	1456	10	Densely welded rhyolitic tuff	NetRS/4000 SSI
SLID	ZBL[b]	2903	10	Weathered granodiorite	NetRS
SLI4	ZBL[b]	2903	10	Weathered granodiorite	4000 SSI

[a]Baseline lengths are relative to site REPO (except SLID and SLI4, which are not at Yucca Mountain). All receivers and antennas were manufactured by Trimble and all antennas are type TRM29659.00, which is a choke ring design. All sites have SCIGN radomes. REP4 had a 4000 SSI receiver from 01/31/07 to 11/31/07, and a NetRS otherwise. Instrumentation given for SLID and SLI4 are for dates after the short-baseline network at Yucca Mountain was installed.
[b]"Zero baseline" (two receivers attached to the same antenna) at Slide Mountain.

error" approach to estimate velocity errors of 0.15 mm/yr for the Yucca Mountain network, and both *Williams et al.* [2004] and *Langbein* [2008] concluded, after examining the noise content of many continuous GPS time series with different monument types and environments, that stations in the southern BARGEN network have the lowest levels of position noise of any stations they examined. *Williams et al.* [2004] estimated, using maximum likelihood estimation, that random walk amplitudes for the BARGEN network are ~ 1.0 mm/yr$^{0.5}$ for the horizontal component and ~ 5.6 mm/yr$^{0.5}$ for the radial. These low levels of noise have been attributed to the fact that this network is almost entirely constructed of deep-braced monuments, fixed into bedrock, with similar or identical equipment at each site. Furthermore, the network is located in a low-humidity, low-precipitation, desert environment. Estimated tectonic rates are also low, at the level of ~ 1 mm/yr over the ~ 60 km width of the Yucca Mountain regional network [*Wernicke et al.*, 2004; *Hill and Blewitt*, 2006].
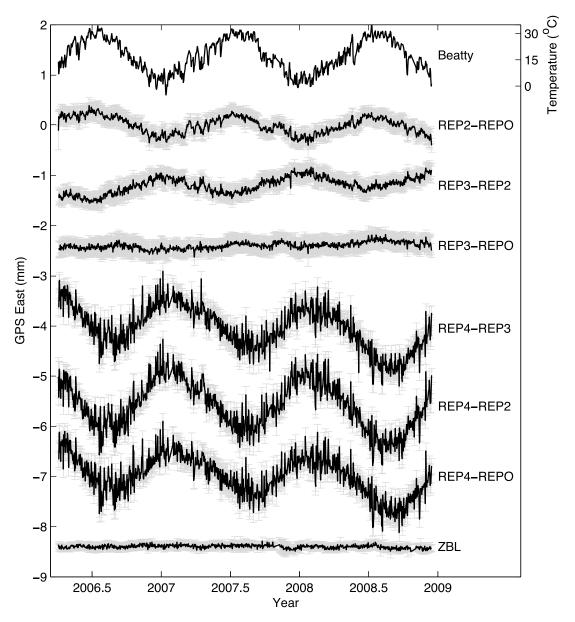
[10] In studies using GPS networks with longer intersite distances it has been difficult to quantify the level to which monument design impacts the accuracy of results. For example, in their study of the noise content of 954 continuous GPS time series, *Williams et al.* [2004] indicated that deep-braced monuments produced the lowest noise levels of all the monument types they examined, but *Beavan* [2005] concluded that the noise properties of the deep-braced monuments in a network in New Zealand were the same as those for the concrete pillars. Sites REPO and REP2 in our network, located just 10 m apart, sample the local motions of essentially the same block of earth, and hence any differences in their motion, in particular higher levels of annual motion or secular drift in REP2 versus REPO, provide a comparison in the performance of the deep- versus short-braced monuments. Understanding differences between shallow- and deep-braced monuments is particularly relevant to the Plate Boundary Observatory (PBO) component of the EarthScope project, which uses a mixture of the two types. We do not know of any other published comparisons of relatively long time series of GPS data acquired by the two different types of monument located in the same place. The high expense of installing high-precision GPS monuments also means that previous studies using deep-braced monuments with very short baselines are relatively few. However, the GPS sites at Piñon Flat Observatory, PIN1 and PIN2, have both very long time series (since 1989), braced monuments, and a short intersite distance of 50 m [*Wyatt and Agnew*, 2005]. The results from these stations have demonstrated that when common sour-

ces of noise cancel out, the remaining baseline scatter is very small [*King and Williams*, 2009].

[11] In addition to GPS data from the short-baseline network at Yucca Mountain, we also use data from the weather station at Beatty, Nevada, located ~ 25 km to the NW of Yucca Mountain (http://www.cemp.dri.edu), and GPS data from two stations (SLID and SLI4) at Slide Mountain, northwest Nevada. The two stations at Slide Mountain receive signals that are split from the same antenna, thus creating a "zero-baseline" (ZBL) network. Since these stations have the same instrumentation as that of the short-baseline stations (Table 1), we can use them to determine lower bounds for the level of receiver or software noise we might expect [*Park et al.*, 2004].

2. GPS Data Processing

[12] We processed the GPS data for our short-baseline network using the GAMIT software package [*Herring et al.*, 2006] and a processing routine adapted for very short baselines. The small linear extent of the network means that many errors with larger spatial scale, and large-scale geophysical signals (or the results of their mismodeling), will be either eliminated or significantly reduced by the double-differencing technique used by GAMIT. We take advantage of this feature in our processing routine, primarily by avoiding the estimation of parameters that will be very similar at all sites. (It would not be possible to achieve the low level of noise we see in our results using a "regular" processing routine with these parameters included.) We did not, therefore, form the "linear combination" (LC) of GPS frequencies to mitigate ionospheric delay. Instead, our site position estimates are based on L1 frequency data only, since these are a factor of ~ 3 more precise than the LC measurements. (Although we did use the L2 frequency data to help resolve cycle slips and fix ambiguities to integer numbers.) Similarly, the satellite orbits were fixed to International GNSS Service (IGS) final orbits, corrections to earth rotation and orientation parameters were not estimated, and we did not apply models for tidal loading. We did resolve integer ambiguities as part of our processing, and because of the short baseline lengths all of the ambiguities were resolved. We used a $10°$ elevation angle cutoff.

[13] We hesitated to include estimation of zenith delay parameters, because over the shortest baselines this will primarily serve to increase the uncertainties. However, the accuracy with which we can potentially estimate relative position (on the order of 0.1 mm for all components) places unusual requirements on our (prior) model for atmospheric

Figure 2. GPS time series for the east component of the baseline vector. For this, and all following time series plots, time series have been offset along the y axis by an arbitrary constant for clarity, error bars are based on 1-σ formal errors, and all baselines are oriented in a north to south direction. The time series labeled ZBL is, for comparison, a baseline time series for the zero-length baseline SLI4-SLID (see text). Temperature data from the Beatty weather station are also shown.

propagation delay if we are not to estimate adjustments to this model. For example, a relative zenith delay error of 0.03 mm will lead to a relative vertical error of ~0.1 mm, depending on observing geometry [e.g., *Herring*, 1986]. Such a zenith delay error can be caused, for example, by an error in the relative ground pressure of ~0.01 mbar. Since we do not make accurate ground pressure measurements, we rely on the Global Pressure and Temperature (GPT) model of *Boehm et al.* [2006] to calculate the pressure at each of the sites. A model error of ~3.5 mbar will lead to an error in the relative pressure between REPO and REP4 of ~0.01 mbar. Additionally, winds of ~15 m/s along the side of Yucca Mountain could lead to a nonhydrostatic contribution to the relative pressure between these two sites of the

same magnitude [*Hauser*, 1989]. We thus conclude that, at these great levels of precision, we do not have enough confidence in our prior atmospheric propagation delay models not to estimate adjustments to the zenith delay. We therefore include zenith delay parameter estimation in our processing, although restrict this to one estimate per site per day to improve our model while not inflating the uncertainties.

[14] We removed all outliers that were 4σ (based on the RMS residuals) from a Gaussian-smoothed profile of the time series. Using this criterion, the only time series that had outliers were those from REP4 (the longest baselines). The maximum number of outliers was 19 for the horizontal components and 3 for the radial (from a total of ~980 data
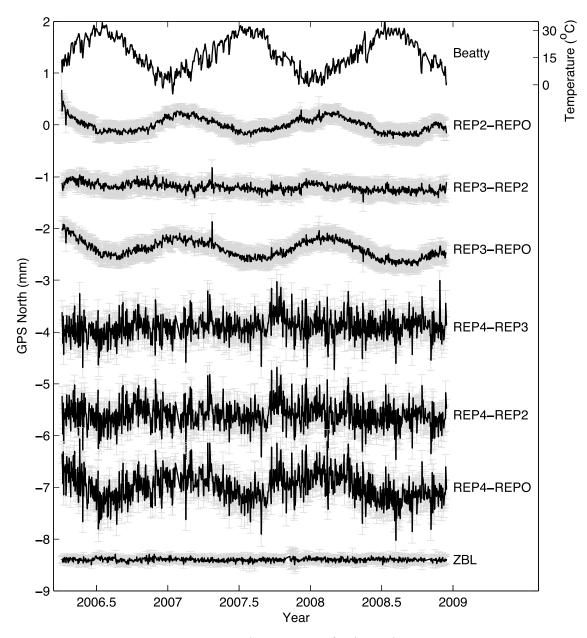
Figure 3. Same as Figure 2 except for the north component.

points). RMS differences between results from a network solution and solutions processed with individual baselines are small: 0.03 mm for the horizontal components and 0.2 mm for the radial. However, more outliers were identified for the individual baseline solutions so the results presented in this paper are from network solutions. All error bars in time series plots are based on 1-σ formal standard deviations, resulting from a phase standard deviation of 10 mm.
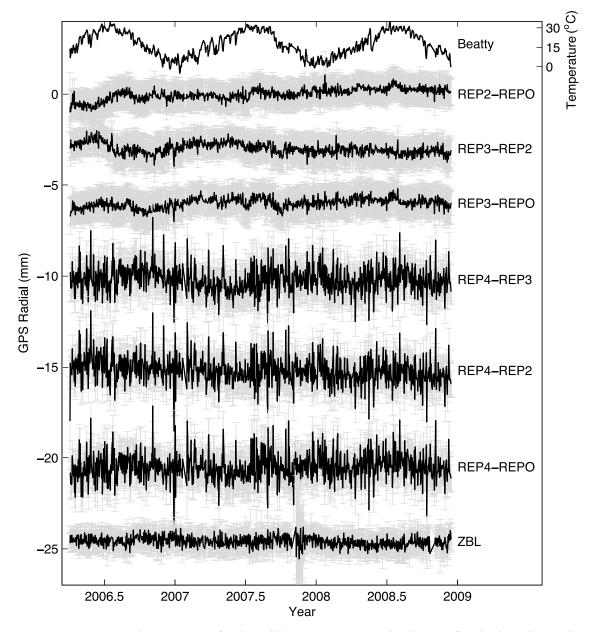
[15] The output from our processing routine was a collection of baseline time series for each station pair and each baseline component in a topocentric system. It is possible to convert these into individual station time series in a local reference frame through the use of suitable constraints. However, the use of a reference frame will always involve some assumptions, and errors at one station may propagate through to the results for other stations. We therefore chose to present our results as baseline time series. This has the disadvantage that we are always working with station pairs

(although redundancy enables us to make some inferences about the individual stations), but the advantage that we avoid any reference frame bias.

3. Results

[16] Time series of baseline vector components are shown in Figures 2–4. Examination of Figures 2–4 reveals that although the time series are extremely stable, the time series do have structure in the form of both seasonal cycles and shorter-period signals. It is also clear that certain time series have a rate. Here we examine these signals in more detail and compare them to data from the Beatty weather station.

3.1. GPS Time Series

[17] Taking the assumption (which is not necessarily accurate) that the periodic cycles in the baseline time series are exactly annual and semiannual, we fit a least squares

Figure 4. Same as Figure 2 except for the radial component. Note the change of scale along the y axis compared to Figures 2 and 3.

model to the time series that included annual, semiannual, and linear terms. Maximum estimated amplitudes (Table 2) for the annual cycles are ∼0.6 mm for the east component, ∼0.2 mm for the north component, and ∼0.2 mm for the radial. Although these amplitudes are very small, they are significant due to the low level of noise in the time series. Spectral analysis (not shown) reveals approximately annual cycles in almost all the time series (exceptions are the REP3-REPO east component, REP3-REP2 north component, and radial component time series not involving REP3), and also a semiannual cycle for baselines to REP4 in the north component.

[18] Certain time series have significant secular rates, with many of the time series having rates ≥0.1 mm/yr. The larger rates are in the east and radial components. The

maximum estimates are −0.3 ± 0.1 mm/yr for the REP4-REP3 east component and 0.3 ± 0.1 mm/yr for the REP2-REPO radial component.

[19] We calculate RMS statistics using residual time series about our model for seasonal cycles and secular rate. Time series for the shortest baselines in our network (REP3-REPO, REPO-REP2, and REP3-REP2) have the smallest RMS values; 0.05–0.07 mm for the horizontal components and 0.20–0.22 for the radial (Table 3). The three longer baselines to REP4 have RMS values that are more than double the size of those for the shorter baselines, although these still only reach a maximum of 0.7 mm for the radial component. Indeed, the RMS values for this network increase quite linearly with baseline length (Figure 5), with a trend of 0.2 ± 0.1 mm/km for the horizontal components

Table 2. Estimated Amplitudes of Annual Cycle for East, North, and Radial Baseline Components[a]

Baseline	Length (m)	Annual Cycle (mm)		
		E	N	R
REP2-REPO	10	0.20 ± 0.01	0.18 ± 0.01	0.03 ± 0.04
REP3-REP2	93	0.17 ± 0.01	0.02 ± 0.01	0.16 ± 0.04
REP3-REPO	103	0.04 ± 0.01	0.19 ± 0.01	0.14 ± 0.04
REP4-REP3	893	0.47 ± 0.01	0.03 ± 0.01	0.20 ± 0.04
REP4-REP2	986	0.60 ± 0.01	0.04 ± 0.01	0.04 ± 0.04
REP4-REPO	996	0.43 ± 0.01	0.21 ± 0.01	0.07 ± 0.04

[a]Component abbreviations are E, east; N, north; and R, radial.

and 0.5 ± 0.2 mm/km for the radial. For comparison, RMS residuals for the ZBL are 0.03 mm for the horizontal components and 0.25 mm for the radial.
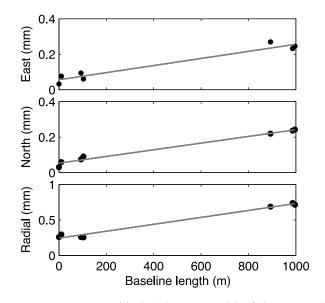
[20] RMS statistics assume white noise. Although we do not carry out a detailed noise analysis (this is a topic for future study, when the time series are longer), use of Maximum Likelihood Estimation (MLE) code from *Langbein* [2004] (in which an annual, semiannual, secular rate, power law index and amplitude, and white noise component are estimated simultaneously) indicates white noise plus noise with characteristics that fall between flicker noise and random walk, with mean power law indices of 1.4 ± 0.2, 1.5 ± 0.2, and 0.9 ± 0.3 for the east, north, and radial components, respectively. (Uncertainties are the standard deviation of values for all baselines.) Assuming white noise plus flicker noise, we estimate white noise amplitudes ranging between 0.02–0.2, 0.03–0.3, and 0.1–0.7 mm for the east, north, and radial components, respectively. Corresponding flicker-noise amplitudes are 0.2–0.5, 0.1–0.9, and 0.1–0.6 mm/yr$^{0.25}$. Assuming white noise plus random walk, random walk amplitudes are on the order of 0.2–0.8 mm/yr$^{0.5}$. For comparison, flicker noise amplitudes for the ZBL results are very small (≤ 0.07 mm/yr$^{0.25}$).

[21] To study effects such as multipath we investigated the results of running the processing with various different minimum elevation angles up to 50°. Regardless of the elevation angle cutoff used, the horizontal time series look quite similar and seasonal cycles remain with similar amplitudes. The RMS difference between a solution with 10° elevation angle cutoff and another with 40° is ~0.1 mm for the horizontal time series, and mean annual cycle amplitudes remain at 0.6 mm and 0.2 mm for the east and north, respectively. Radial component time series have increasing levels of noise as elevation angle cutoff values are increased (e.g., for a 10° elevation angle cutoff the mean RMS for the radial time series is 0.5 mm, while for 40° it is

Table 3. RMS Residual About a Model That Includes Seasonal Cycles and a Linear Term[a]

Baseline	East	North	Radial
REP2-REPO	0.07	0.06	0.20
REP3-REP2	0.06	0.06	0.24
REP3-REPO	0.05	0.06	0.22
REP4-REP3	0.18	0.22	0.68
REP4-REP2	0.20	0.24	0.72
REP4-REPO	0.18	0.24	0.71
ZBL	0.03	0.03	0.25

[a]RMS residual is in units of mm. Seasonal cycles are annual and semiannual. Baseline lengths are given in Table 2, except for ZBL which is 0 m.

Figure 5. RMS residuals (about a model of the seasonal cycle and linear term) for the GPS time series, as a function of baseline length. Note the change of scale, along the y axis, for the radial component.

3.5 mm), so it is not possible to tell if the seasonal cycles in the radial time series are reduced. The time series from these different solutions are systematically offset from each other. This is true for all baseline components, but the largest offsets occur for the radial component (e.g., maximum offset for the horizontal component, between solutions with 5 and 40° elevation angle cutoffs, is 0.2 mm while for the radial it is 9 mm). This implies some level of multipath. However, the pattern of these offsets is different for each baseline, with some offsets becoming increasingly positive with increasing elevation angle cutoff and others more negative. There is no one station that produces particularly large offsets compared to the others.

[22] We also investigated the results of a solution that uses the LC observations to allow for ionospheric delay variations. These solutions are considerably noisier, as expected, and many of the signals seen in the L1-only solutions are obscured by this. Seasonal cycles still occur in the time series for the longer baselines and are not significantly reduced. The mean RMS for horizontal components increases from 0.1 to 0.2 mm, and for the vertical mean RMS increases from 0.5 to 0.8 mm.

[23] The main effect of including the estimation of zenith delay parameters for the shortest baselines will be to increase the uncertainties and scatter in the time series. We therefore also examined solutions that were produced without these additional parameters. For the horizontal components the time series are almost identical. However, for the radial component significant seasonal cycles are introduced to the results for the longer baselines when zenith delay estimation is omitted (mean amplitudes increase from 0.1 with zenith delay estimation to 0.8 mm without), illustrating the importance of accurate prior atmospheric delay models even over 1 km. The RMS residual (calculated about these seasonal cycles) is significantly decreased for the shorter baseline radial time series, when zenith delay parameters are omitted, from a mean of 0.2 mm

Table 4. Estimated Phase Difference Between Annual Cycles for GPS and Temperature Data for East, North, and Radial Components[a]

	Phase Difference (days)		
Baseline	E	N	R
REP2-REPO	5 ± 3	−35 ± 2	–
REP3-REP2	9 ± 4	–	–
REP3-REPO	–	−33 ± 2	1 ± 13
REP4-REP3	−33 ± 1	–	−43 ± 1
REP4-REP2	−23 ± 1	–	−35 ± 1
REP4-REPO	−35 ± 1	−24 ± 3	−38 ± 1

[a]Component abbreviations are E, east; N, north; and R, radial. Missing values indicate that the estimated amplitude of the GPS annual cycle was ≤0.1 mm. Negative numbers indicate that the GPS annual cycles lag those of the temperature.
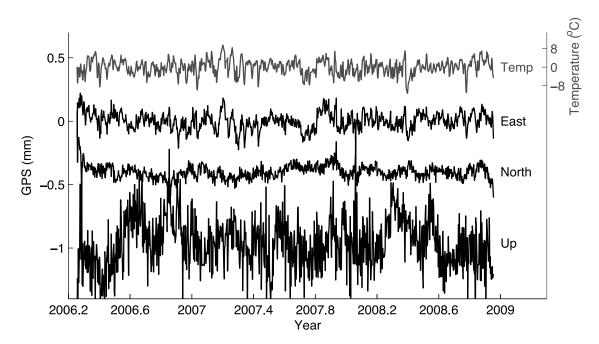
to a mean of 0.1 mm. Similarly, the RMS residual for the ZBL radial time series is reduced from 0.25 to 0.07 mm.
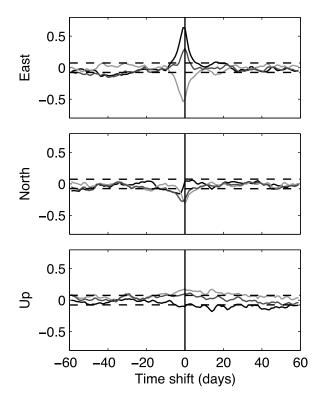
3.2. Comparison With Weather Data

[24] A visual comparison of the temperature data with the GPS results (Figures 2–4) reveals that the seasonal signals are approximately in phase. Although all the baselines are ordered to go from north to south, there is a mix of negative and positive correlations between the GPS and temperature annual cycles. We also see that some of the shorter-period signals appear to be correlated.

[25] Table 4 illustrates the difference in phase between models of an annual cycle through the GPS and temperature data. For the time series that have significant seasonal cycles, the GPS annual cycles lag those of the temperature by 23–43 days, with uncertainties of 1–3 days. However, for the REP2-REPO and REP3-REP2 baselines in the east component, the GPS precedes the temperature by a very small phase shift of ∼7 ± 4 days. Quoted uncertainties are

based on the propagation of the GPS formal errors and an assumed uncertainty of 3.2 °C for the temperature data (based on the RMS residuals after fitting a seasonal cycle). Since these a priori sigma values may be underestimated, and we also consider that these cycles may not be exactly annual, the phase uncertainties may also be underestimated and we therefore do not consider this small lead to indicate a lack of causality. Rather, there seems to be a more direct relationship between temperature and position changes for the two short baselines to REP2 in the east component, while the other horizontal time series may be related but with a lag time.

[26] To investigate the shorter-period signals in the data we removed the models for seasonal cycle from both the temperature and GPS time series (e.g., Figure 6). Correlations are seen primarily in the east component and are highest for baselines to REP2, with a correlation coefficient of 0.6 for the REP2-REPO baseline and −0.5 for REP3-REP2. These are the same time series that indicated no lag time between GPS and temperature seasonal cycles. Cross-correlation analysis indicates that there is also no lag time (or perhaps a 1 day lag) between the temperature and GPS shorter-period signals (e.g., Figure 7). Correlations for the north and radial components are marginally significant or uncorrelated, with the most significant correlation for these components being −0.3 for the REP3-REP2 north component (the 99% confidence interval is estimated to be ∼0.1). Similarly, correlations for east time series not involving REP2 are only marginally correlated (e.g., 0.3 for the REP3-REPO time series). These also have no significant lag time. As discussed, omitting zenith delay parameters in the processing reduces the noise in the shorter baseline radial time series. Correlations in the radial for these time series are slightly higher (e.g., 0.3 for the REP3-REP2 baseline). Correlations calculated using time series that have had

Figure 6. Shorter-period signals (residuals after removing a model for the seasonal cycle) for the temperature and REP2-REPO time series (the shortest, ∼10 m, baseline). For illustration purposes, the time series have been offset along the y axis.

Figure 7. Example cross-correlation plots for residual temperature and GPS time series (after a model for the seasonal cycle has been removed). The plots show results for the shortest baselines, with REP2-REPO shown in black, REP3-REP2 shown in light gray and REP3-REPO in dark gray. The dotted line represents the 99% confidence level.

longer-period signals removed using a Gaussian-filtered time series, rather than a model for the seasonal cycle, are also slightly higher (e.g., 0.7 for the REP2-REPO east component).

[27] We estimated a scaling factor to fit the residual temperature data (seasonal cycles removed) to the most significantly correlated GPS residuals (REP2-REPO in the east component). This scaling factor is estimated to be ~0.01 mm/°C. Removal of this scaled temperature time series from the GPS residuals results in a time series with RMS of 0.05 mm (a reduction of 0.02 mm).

[28] We also examined precipitation data from the Beatty weather station. The level of precipitation is very low: Mean total annual precipitation was ~8 cm. There is no clear seasonal cycle in the precipitation data. Rainfall events are sporadic, and we do not see a clear pattern between these events and the GPS results. Correlation coefficients calculated between the GPS and precipitation data (with an exponential decay pattern applied to each rainfall event to approximate soil moisture) reveal small correlations of up to ~0.25 (with a 99% confidence level of ~0.1). It is therefore possible that there is some relationship between precipitation and the GPS results, but it is not strong.

[29] We note that the Beatty weather station is ~25 km from Yucca Mountain, so there could be differences in the data observed here and the actual temperature and precipitation values at Yucca Mountain. There is a weather station at Yucca Mountain itself (YMP2, http://ymp.dri.edu), but unfortunately the data for this station are only available until the end of 2006 (at the time of this writing). However, comparison of data from 1999 to 2006 for the two stations reveals that the these data are very similar to that from Beatty. For example, the correlation between temperature measurements from the two locations is 0.98, or 0.90 with the seasonal cycles removed, and the precipitation data have a correlation coefficient of 0.74. The elevation difference between the two stations is 396 m (we applied no correction for this when calculating correlations).

4. Discussion

[30] Results from the ZBL indicate RMS noise of 0.03 mm. This is 50%, or more, of the RMS residuals for the shorter baselines in our network. However, the short-baseline residuals are calculated about some significant seasonal cycles and there are remaining shorter-period signals to be explained. Seasonal cycles in many of the time series lag those in local temperature records by up to one month. Seasonal cycles for shorter-period signals and seasonal cycles for the shortest baselines to REP2, in the east component, have a dependency with temperature that has no lag time. In this section we discuss possible effects related to thermal expansion, both of the mountain, the upper ground layers, and the monuments themselves. We show that multipath is unlikely to be the primary cause of the seasonal cycles in the horizontal time series. We also discuss possible causes for a baseline length dependency in the level of noise in the time series.

4.1. Thermal Expansion

[31] We estimated an approximate lag time of 23–43 days between the seasonal cycles for GPS and temperature in many time series, and hypothesize that these could be related to bedrock thermal expansion. Similar phase delays between temperature and GPS were estimated by *Dong et al.* [2004] and observed in SCIGN GPS time series by *Prawirodirdjo et al.* [2006]. Although our network is so small that we might assume that all stations would undergo a similar level of displacement as a result of bedrock thermal expansion (that would then cancel as a common mode signal) it is possible that there are small differences. For example, Yucca Mountain is a typical Basin and Range-style tilted fault block, with a steep cliff to the west and a more gradual slope to the east (Figure 1). Differences between the sites in their proximity to the cliff, differences in the exact orientation of the cliff at the location of each site, or differences in geology at each location (e.g., depth of the unconsolidated upper layer [*Ben-Zion and Leary*, 1986]), could modify the response at each site to thermal expansion.

[32] For the shorter-period correlated signals, and seasonal cycles which have no lag time (primarily seen in the shorter east baseline time series to REP2), we suspect a more local source of deformation. As discussed previously, differences in the results for REP2 (the only short-braced monument) and the nearby deep-braced monuments should reflect processes occurring in the upper few meters of the ground. As shown by *Ben-Zion and Leary* [1986], crustal temperature variations are delayed, attenuated, and low-pass filtered with depth through the upper ground layers. It is, therefore, not unlikely that short-period temperature variations would be seen to affect the REP2 time series but not

the other deep-braced monuments, and that while temperature effects at the deeper monuments are delayed, this is not the case for the shallower monument.

[33] We also note, however, that small, marginally significant, correlations were also observed between the short-period signals and the baselines not involving REP2, and we are not able to explain why signals are observed for some baselines in the east component and others in the north. We also, therefore, consider the idea that thermal expansion of the monuments themselves could cause the shorter-period signals in the GPS. Variations in the local topography mean that the exposed length (from the top of the insulating pipe to the center point of the weld contact with the vertical post) of some legs are slightly longer than others. The maximum difference in slanted leg length is ~15 cm. The orientation of the legs is similar, but not identical, for all sites (Figure S2 in the auxiliary material). Although the majority of monument thermal expansion would occur in the radial direction (and then mostly cancel as a common mode signal), we also hypothesize that horizontal signals may occur as a result of differences in the length or orientation of the monument legs. Furthermore, the monument legs for the deep-braced monuments are hollow, 3.2 cm diameter, galvanized steel pipes filled with rebar and grout, whereas the legs for the shallow-braced monument are solid, 2.5 cm diameter, stainless steel rods. These differences may also contribute to differences in the response of the deep- versus shallow-braced monuments to changes in temperature.

4.2. Multipath

[34] The stations at Yucca Mountain have choke ring antennas that somewhat reduce the effects of multipath, and there are no buildings or trees in this area. However, a number of reflectors do exist around the antennas, including the solar panels and receiver boxes that are present at each station, and, obviously, the ground itself. Attempts were made to make the station setup configurations as similar as possible, but station REPO is surrounded by a chain-link fence that is not present at the other sites. It is therefore likely that multipath will affect the daily position estimates at some level, and this level may vary between stations.

[35] Multipath is more likely to affect signals that arrive at the receiver from low elevation angles, so the use of a higher elevation angle cutoff value might be expected to modify any effects of multipath [e.g., *Elósegui et al.*, 1995]. As we noted in section 3.1, annual cycles in the horizontal components are similar regardless of the elevation angle cutoff used, suggesting that multipath is not a significant contributor to these. Time series are also, however, increasingly offset from each other with increasing elevation angle cutoff, indicating the possibility of consistent sources of multipath, and small differences in the time series may indicate the presence of shorter-period sources. The radial time series become increasingly noisy with increased elevation cutoff angle, so we were unable to assess the effects of multipath on the radial component using these tests. Using the considerably less noisy time series produced without zenith delay parameter estimation introduces the problem that any differences in tropospheric delay will also be absorbed by using higher elevation angle cutoffs (while, conversely, the estimated zenith delay parameters may

absorb the effects of multipath). Despite the chain-link fence at station REPO, we do not see significant differences between baselines to this station and other baselines in the elevation angle cutoff plots.

4.3. Monument Wander

[36] *Williams et al.* [2004] estimated white noise plus flicker noise (versus white noise plus random walk) to be the preferred model for BARGEN sites. *Langbein* [2008] confirmed flicker noise to be a preferred model over random walk. Our limited noise analysis indicates power law indices somewhere between flicker noise and random walk, although we note the short time series lengths. Our estimates for power law index (1.4 ± 0.2, 1.5 ± 0.2, and 0.9 ± 0.3 for the east, north, and radial components, respectively) are just slightly higher than those from *Williams et al.* [2004] for the BARGEN network (1.0 ± 0.4, 1.4 ± 0.4, and 0.9 ± 0.4 for the east, north, and radial), and those from *Langbein* [2008] (1.1 ± 0.4, 1.0 ± 0.5, and 1.0 ± 0.3, for the east, north, and radial).

[37] *Williams et al.* [2004] estimated white noise amplitudes for the BARGEN sites of 0.7 ± 0.2, 0.5 ± 0.1, and 2.2 ± 0.5 mm for the east, north, and radial, with flicker noise amplitudes of 1.2 ± 0.7, 1.2 ± 0.4, and 5.4 ± 3.1 mm/yr$^{0.25}$. *Langbein* [2008] estimated similar white noise amplitudes to *Williams et al.* [2004] and slightly lower flicker noise amplitudes (0.9 ± 0.2, 0.8 ± 0.3, and 3.6 ± 1.1 mm/yr$^{0.25}$ for the east, north, and radial). It is clear that the level of repeatability for our short-baseline results is considerably smaller than these previous noise estimates for BARGEN stations. Assuming white noise plus flicker noise we estimate white noise amplitudes of ≤ 0.3 mm for the horizontal components, with some values as low as 0.02 mm, and ≤ 0.7 mm for the radial. Corresponding flicker noise amplitudes are a maximum of 0.9 mm/yr$^{0.25}$, with many time series at the level of 0.1 mm/yr$^{0.25}$.

[38] Although it was not their preferred noise model, *Williams et al.* [2004] also estimated nominal values for random walk noise at BARGEN sites of 1.0, 1.0, and 5.6 mm/yr$^{0.5}$. It is clear that any random walk component that does exist in our time series is unlikely to occur on these levels. It is likely, as they state in their paper, that the numbers estimated by *Williams et al.* [2004] reflect not only monument noise, but also other sources of noise caused by the fact that their data was processed as a large regional network (e.g., unmodeled atmospheric effects). If random walk does exist in our network, our noise levels seem to be more consistent with the short-baseline results from the Piñon Flat Observatory, for which estimated random walk noise is ~0.1–0.3 mm/yr$^{0.5}$ (see from S. D. P. Williams (personal communication, 2004) as cited by *Beavan* [2005]). Similar values for random walk amplitude have also been estimated for other short baselines [*King and Williams*, 2009].

[39] Our network is only sensitive to motions of the very local area around the monuments. For this very local area we do not appear to be measuring significant monument wander. However, we are currently insensitive to motions involving, for example, the rest of the mountain, which could also be included in a definition of "monument wander." In other words, the entire network could be wandering over time, and without the addition of more

distant sites (a topic for future research) we would not see this.

[40] Estimated secular rates for this network were surprisingly large for many time series. Although the estimated rates could be related to tectonics they are quite large compared with previous estimates of fault activity for the Yucca Mountain area. For example, a rate of 0.2 mm/yr over a 1 km baseline produces a strain rate of 200 ns/yr, which is very high; previously estimated strain rates have been on the order of ~20 ns/yr [*Wernicke et al.*, 2004; *Hill and Blewitt*, 2006]. It is possible that these rates are, instead, showing the results of longer-term monument wander. Another possibility might be the effect of systematic errors related to the aging of the equipment.

[41] We do not see a significant difference in the RMS values for baselines to REP2, the shallow-braced station, compared with those for baselines between deep-braced sites, nor do we see significant differences in our estimate of the power law index. This suggests that it is possible to obtain extremely high-precision measurements from shallow, as well as deep, braced monuments. However, we do see higher correlations between the results from this station and the temperature data, suggesting that local environment could play a role in determining the precision of results from shallow-braced monuments, compared with those from deep-braced monuments. Moreover, although rates for baselines to this station are relatively small for the horizontal components, they are higher (by up to 0.1 mm/yr) for the radial components, compared to baselines to other stations. We also note that this monument is installed into bedrock, so is likely to be considerably more stable than similar sites installed into alluvium. In general, the dry environment at Yucca Mountain may be a contributing factor to the high levels of site stability that we observe at this network. For example, *Wyatt* [1982, 1989] found precipitation to be a dominating influence on levels of monument displacements in their tiltmeter and strainmeter tests at Piñon Flat Observatory. *Langbein* [2008] also found a correlation, for ~200 GPS sites in California and Nevada, between average annual rainfall at a site and its standard error in rate for the north component (the east and vertical components had only a weak dependence).

4.4. Baseline Length-Dependent Effects

[42] RMS residuals increase with baseline length, with RMS residuals for baselines to REP4 double those for the shorter baselines. Since baselines to REP4 are an order of magnitude further from the other stations (~1 km), those errors that we assumed would cancel (e.g., satellite orbit errors) may factor into our results for these baselines (although we cannot rule out the possibility of site-specific sources of noise at REP4 being independently larger than those at the other sites).

[43] Errors in the satellite orbits (we used IGS final orbits with an estimated accuracy of ≤5 cm (http://igscb.jpl.nasa.gov/components/prods.html, 2007)) could result in an ~0.002 mm position error over a 1000 m baseline, and antenna phase center variations (PCVs) could result in an error of 0.015 mm (although the antennas are all the same type, they could experience PCVs as a result of "seeing" satellites with difference elevation angles [*Rothacher et al.*, 1995]). Although these do not seem to be large enough to

account for the larger RMS values for baselines to REP4 by themselves, they may well contribute.

[44] We indicated in sections 2 and 3.1 that even small differences in atmospheric delay could have significant implications for results with such high levels of precision. Although we estimate zenith delay parameters, we do not estimate each temporal variation, nor tropospheric gradients. Small differences in atmospheric symmetry could therefore be impacting the results for the longer baselines. The study of propagation delay over such small baseline lengths is an area for continuing study. For example, *Nilsson et al.* [2009] demonstrate that variability of zenith total delay estimates for the Yucca Mountain GPS network, which includes our short-baseline network and surrounding stations, can be approximated quite well using Kolmogorov turbulence theory.

[45] We found that the results have an elevation angle dependence. There is a systematic offset between time series from solutions with increasing values for the elevation angle cutoff. A baseline-dependent multipath effect could also, therefore, be possible.

[46] The higher levels of noise at REP4 may illustrate the much greater impact of baseline length on the stability of a solution than the impact of site-specific errors. This network has been designed so that additional baselines to BARGEN stations at ~10^4, 10^5 and 10^6 m from Yucca Mountain will allow us to investigate baseline-dependent errors at a full 6 orders of magnitude. This is a topic for further work.

5. Conclusions

[47] The results from this study place the upper bounds for RMS noise at these sites, over 2.7 years, at ~0.2 mm for the horizontal components and ~0.7 mm for the radial. For the shortest baselines, the RMS values are as low as 0.05 mm for the horizontal components, with ~50% of this likely to be attributable to receiver noise. This suggests that results from other similar stations, in similar environments (which would include many of the PBO sites and much of the BARGEN network), are unlikely to be significantly affected by local processes. This also suggests that, for similar stations, errors with a larger spatial extent (e.g., unmodeled atmospheric effects) are likely to be a far greater source of noise in the GPS results.

[48] Seasonal cycles occur in the time series, with amplitudes ≤0.6 mm. These occur even in the horizontal components and even for the shortest baselines. Even with their relatively small magnitude, these seasonal signals are clearly distinguishable due to the low level of noise in the time series. This is not an isolated case; seasonal cycles have also been seen in the time series for other short baselines [*King and Williams*, 2009].

[49] Seasonal cycles for many time series have an estimated lag time of up to 1 month behind seasonal cycles in local temperature data, with bedrock thermal expansion a possible cause. Shorter-period signals, particularly for baselines to REP2 in the east component, are also correlated with temperature, however these do not have a lag. Seasonal cycles for REP2 east baselines also have no lag behind the seasonal cycles in temperature data. Since REP2 is the only short-braced monument in the network, baselines to this station will exclusively see processes occurring in the upper

few meters of the ground. While temperature effects will be low-pass filtered and delayed with depth to the deep-braced monuments, this may not be the case for REP2, which could explain the difference in reaction to changes in temperature. An alternative hypothesis is that the signals could be reflecting thermal expansion of the monuments themselves (e.g. REP2 has solid legs while the other monuments have hollow legs). Detailed models and additional tests, that are beyond the scope of this paper, would be required to prove which, if any, of these processes are most important.

[50] Multipath does not appear to be a cause of the seasonal signals in the horizontal components, since these do not reduce with increasing elevation angle cutoff. We do, however, see an elevation angle dependency in the systematic offset between time series with different cutoff values.

[51] Despite the higher correlation with temperature, noise levels for baseline time series to the shallow-braced monument are not significantly different to those using only deep-braced monuments, suggesting that extremely high-precision results can be obtained at both shallow- and deep-braced stations, at least in an environment such as these sites are located.

References

Axelrad, P., C. J. Comp, and P. F. MacDoran (1996), SNR-based multipath error correction for GPS differential phase, *IEEE Trans. Aerosp. Electron. Syst.*, *32*(2), 650–660, doi:10.1109/7.489508.

Baueršíma, I. (1983), NAVSTAR/Global positioning System (GPS), *Mitt. Satelliten-Beobachtungsstn. Zimmerwald 7*, Druckerei, Univ. Bern, Bern.

Bawden, G. W., W. Thatcher, R. S. Stein, K. W. Hudnut, and G. Peltzer (2001), Tectonic contraction across Los Angeles after removal of groundwater pumping effects, *Nature*, *412*, 812–815, doi:10.1038/35090558.

Beavan, J. (2005), Noise properties of continuous GPS data from concrete pillar geodetic monuments in New Zealand and comparison with data from U.S. deep drilled braced monuments, *J. Geophys. Res.*, *110*, B08410, doi:10.1029/2005JB003642.

Ben-Zion, Y., and P. Leary (1986), Thermoelastic strain in a half-space covered by unconsolidated material, *Bull. Seismol. Soc. Am.*, *76*(5), 1447–1460.

Boehm, J., R. Heinkelmann, and H. Schuh (2006), A global model of pressure and temperature for geodetic applications, *J. Geod.*, *81*(10), 679–683, doi:10.1007/s00190-007-0135-3.

Davis, J. L., T. A. Herring, I. I. Shapiro, A. E. E. Rogers, and G. Elgered (1985), Geodesy by radio interferometry: Effects of atmospheric modeling errors on estimates of baseline length, *Radio Sci.*, *20*(6), 1593–1607, doi:10.1029/RS020i006p01593.

Davis, J. L., R. A. Bennett, and B. P. Wernicke (2003), Assessment of GPS velocity accuracy for the Basin and Range Geodetic Network (BARGEN), *Geophys. Res. Lett.*, *30*(7), 1411, doi:10.1029/2003GL016961.

Davis, J. L., B. L. Wernicke, S. Bisnath, N. A. Niemi, and P. Elósegui (2006), Subcontinental-scale crustal velocity changes along the Pacific-North America transform plate boundary from BARGEN GPS data, *Nature*, *441*, 1131–1134, doi:10.1038/nature04781.

Dong, D., P. Fang, Y. Bock, M. K. Cheng, and S. Miyazaki (2002), Anatomy of apparent seasonal variations from GPS-derived site position time series, *J. Geophys. Res.*, *107*(B4), 2075, doi:10.1029/2001JB000573.

Dragert, H., K. Wang, and T. S. James (2001), A silent slip event on the deeper Cascadia subduction interface, *Science*, *292*, 1525–1528, doi:10.1126/science.1060152.

Elósegui, P., J. L. Davis, R. T. K. Jaldehag, J. M. Johansson, A. E. Niell, and I. I. Shapiro (1995), Geodesy using the Global Positioning System: The effects of signal scattering on estimates of site position, *J. Geophys. Res.*, *100*(B6), 9921–9934, doi:10.1029/95JB00868.

Finnegan, N. J., M. E. Pritchard, R. B. Lowman, and P. R. Lundgren (2008), Constraints on surface deformation in the Seattle, WA, urban corridor from satellite radar interferometry time-series analysis, *Geophys. J. Int.*, *174*, 29–41, doi:10.1111/j.1365-246X.2008.03822.x.

Freed, A. M., R. Bürgmann, and T. Herring (2007), Far-reaching transient motions after Mojave earthquakes require broad mantle flow beneath a strong crust, *Geophys. Res. Lett.*, *34*, L19302, doi:10.1029/2007GL030959.

Hauser, J. (1989), Effects of deviations from hydrostatic equilibrium on atmospheric corrections to satellite and lunar laser range measurements, *J. Geophys. Res.*, *94*(B8), 10,182–10,186, doi:10.1029/JB094iB08p10182.

Herring, T. A. (1986), Precision of vertical position estimates from very long baseline interferometry, *J. Geophys. Res.*, *91*(B9), 9177–9182, doi:10.1029/JB091iB09p09177.

Herring, T. A., R. W. King, and S. C. McClusky (2006), GAMIT reference manual, release 10.3, Dep. of Earth, Atmos., and Planet. Sci., Mass. Inst. of Technol., Cambridge. (Available at http://chandler.mit.edu/simon/gtgk/GAMIT_Ref_10.3.pdf)

Hill, E. M., and G. Blewitt (2006), Testing for fault activity at Yucca Mountain, Nevada, using independent GPS results from the BARGEN network, *Geophys. Res. Lett.*, *33*, L14302, doi:10.1029/2006GL026140.

Johnson, H. O., and D. C. Agnew (1995), Monument motion and measurements of crustal velocities, *Geophys. Res. Lett.*, *22*(21), 2905–2908, doi:10.1029/95GL02661.

Kedar, S., G. A. Hajj, B. D. Wilson, and M. B. Heflin (2003), The effect of the second order GPS ionospheric correction on receiver positions, *Geophys. Res. Lett.*, *30*(16), 1829, doi:10.1029/2003GL017639.

King, M. A., and S. D. P. Williams (2009), Apparent stability of GPS monumentation from short-baseline time series, *J. Geophys. Res.*, *114*, B10403, doi:10.1029/2009JB006319.

King, M. A., C. S. Watson, N. T. Penna, and P. J. Clarke (2008), Subdaily signals in GPS observations and their effect at semiannual and annual periods, *Geophys. Res. Lett.*, *35*, L03302, doi:10.1029/2007GL032252.

Langbein, J. (2004), Noise in two-color electronic distance meter measurements revisited, *J. Geophys. Res.*, *109*, B04406, doi:10.1029/2003JB002819.

Langbein, J. (2008), Noise in GPS displacement measurements from southern California and southern Nevada, *J. Geophys. Res.*, *113*, B05405, doi:10.1029/2007JB005247.

Langbein, J., and H. Johnson (1997), Correlated errors in geodetic time series: Implications for time-dependent deformation, *J. Geophys. Res.*, *102*(B1), 591–603, doi:10.1029/96JB02945.

Langbein, J., R. O. Burford, and L. E. Slater (1990), Variations in fault slip and strain accumulation at Parkfield, California: Initial results using two-color geodimeter measurements, 1984–1988, *J. Geophys. Res.*, *95*(B3), 2533–2552, doi:10.1029/JB095iB03p02533.

Larson, K. M., P. Bodin, and J. Gomberg (2003), Using 1-Hz GPS data to measure deformations caused by the Denali Fault earthquake, *Science*, *300*, 1421–1424, doi:10.1126/science.1084531.

Larson, K. M., E. E. Small, E. Gutmann, A. Bilich, P. Axelrad, and J. Braun (2008), Using GPS multipath to measure soil moisture fluctuations: Initial results, *GPS Solut.*, *12*, 173–177, doi:10.1007/s10291-007-0076-6.

Lowry, A. R., K. M. Larson, V. Kostoglodov, and R. Bilham (2001), Transient fault slip in Guerrero, southern Mexico, *Geophys. Res. Lett.*, *28*(19), 3753–3756, doi:10.1029/2001GL013238.

Mao, A., C. G. A. Harrison, and T. H. Dixon (1999), Noise in GPS coordinate time series, *J. Geophys. Res.*, *104*(B2), 2797–2816, doi:10.1029/1998JB900033.

Nilsson, T., J. L. Davis, and E. M. Hill (2009), Using ground-based GPS to characterize atmospheric turbulence, *Geophys. Res. Lett.*, *36*, L16807, doi:10.1029/2009GL040090.

Ozawa, S., S. Miyazaki, Y. Hatanaka, T. Imakiire, M. Kaidzu, and M. Murakami (2003), Characteristic silent earthquakes in the eastern part of the Boso peninsula, central Japan, *Geophys. Res. Lett.*, *30*(6), 1283, doi:10.1029/2002GL016665.

Park, K.-D., P. Elósegui, J. L. Davis, P. O. J. Jarlemark, B. E. Corey, A. E. Niell, J. E. Normandeau, C. E. Meetens, and V. A. Andreatta (2004), Development of an antenna and multipath calibration system for Global Positioning System sites, *Radio Sci.*, *39*, RS5002, doi:10.1029/2003RS002999.

Penna, N. T., M. A. King, and M. P. Stewart (2007), GPS height time series: Short-period origins of spurious long-period signals, *J. Geophys. Res.*, *112*, B02402, doi:10.1029/2005JB004047.

Prawirodirdjo, L., Y. Ben-Zion, and Y. Bock (2006), Observation and modeling of thermoelastic strain in Southern California Integrated GPS Network daily position time series, *J. Geophys. Res.*, *111*, B02408, doi:10.1029/2005JB003716.

Ray, J., Z. Altamimi, X. Collilieux, and T. van Dam (2007), Anomalous harmonics in the spectra of GPS position estimates, *GPS Solut.*, *12*(1), 55–64, doi:10.1007/s10291-007-0067-7.

Romagnoli, C., S. Zerbini, L. Lago, B. Richter, D. Simon, F. Domenichini, C. Elmi, and M. Ghirotti (2003), Influence of soil consolidation and thermal expansion effects on height and gravity variations, *J. Geodyn.*, *35*, 521–539, doi:10.1016/S0264-3707(03)00012-7.

Rothacher, M., S. Schaer, L. Mervart, and G. Beutler (1995), Determination of antenna phase center variations using GPS data, in *IGS Workshop Proceedings: Special Topics and New Directions*, edited by G. Gendt and G. Dick, pp. 205–220, GeoForschungsZentrum Potsdam, Germany.

Treuhaft, R. N., and G. E. Lanyi (1987), The effect of the dynamic wet troposphere on radio interferometric measurements, *Radio Sci.*, *22*(2), 251–265, doi:10.1029/RS022i002p00251.

Wernicke, B., A. M. Friedrich, N. A. Niemi, R. A. Bennett, and J. L. Davis (2000), Dynamics of plate boundary fault systems from Basin and Range Geodetic Network (BARGEN) and geologic data, *GSA Today*, *10*(11), 1–7.

Wernicke, B., J. L. Davis, R. A. Bennett, J. E. Normandeau, A. M. Friedrich, and N. A. Niemi (2004), Tectonic implications of a dense continuous GPS velocity field at Yucca Mountain, Nevada, *J. Geophys. Res.*, *109*, B12404, doi:10.1029/2003JB002832.

Williams, S. D. P., Y. Bock, P. Fang, P. Jamason, R. M. Nikolaidis, L. Prawirodirdjo, M. Miller, and D. J. Johnson (2004), Error analysis of continuous GPS position time series, *J. Geophys. Res.*, *109*, B03412, doi:10.1029/2003JB002741.

Wyatt, F. K. (1982), Displacement of surface monuments: Horizontal motion, *J. Geophys. Res.*, *87*(B2), 979–989, doi:10.1029/JB087iB02p00979.

Wyatt, F. K. (1989), Displacement of surface monuments: Vertical motion, *J. Geophys. Res.*, *94*(B2), 1655–1664, doi:10.1029/JB094iB02p01655.

Wyatt, F. K., and D. C. Agnew (2005), The PIN1 and PIN2 GPS Sites at Pinon Flat Observatory, *Tech. Rep. 33*, Scripps Inst. of Oceanogr., La Jolla, Calif. (Available at http://repositories.cdlib.org/sio/techreport/33)

Zhang, J., Y. Bock, H. Johnson, P. Fang, S. Williams, J. Genrich, S. Wdowinski, and J. Behr (1997), Southern California Permanent GPS Geodetic Array: Error analysis of daily position estimates and site velocities, *J. Geophys. Res.*, *102*(B8), 18,035–18,055, doi:10.1029/97JB01380.

———————————

J. L. Davis, E. M. Hill, and E. Malikowski, Harvard-Smithsonian Center for Astrophysics, 60 Garden St., MS 42, Cambridge, MA 02138, USA. (jdavis@cfa.harvard.edu; ehill@cfa.harvard.edu; emalikowski@cfa.harvard.edu)

P. Elósegui, Institute for Space Sciences, CSIC/IEEC, E8034 Barcelona, Spain. (pelosegui@ice.csic.es)

N. A. Niemi, Department of Geological Sciences, University of Michigan, 2534 CC Little Bldg, 1100 North University Ave., Ann Arbor, MI 48109, USA. (naniemi@umich.edu)

B. P. Wernicke, Division of Geological and Planetary Sciences, California Institute of Technology, Pasadena, CA 91125, USA. (brian@gps.caltech.edu)